A Reconfigurable Surface Acoustic Wave Filter on ZnO/AlGaN/GaN Heterostructure

José A. Bahamonde *Student Member, IEEE*, and Ioannis Kymissis, *Senior Member, IEEE*

***Abstract*— With the increasing number of filters on radio frequency front ends, especially in hand held systems such as cell phones, there has been a growing interest developing reconfigurable filters to accommodate all of the frequencies used modern communication protocols. This article demonstrates a voltage tunable filter by utilizing the acoustoelectric effect between acoustic waves on Zinc Oxide (ZnO) and the two-dimensional electron gas (2DEG) in the interface of Aluminum Gallium Nitride (AlGaN) and Gallium Nitride (GaN). The device is capable of tuning the center frequency by up to 0.78%. Furthermore, the emergence of an accumulation region at the ZnO/AlGaN interface allows for control of the side-band rejection ratio by 16 dB and bandwidth by 12 dB demonstrating a degree of reconfigurability previously not reported.**

***Index Terms*— Acoustoelectric Effect, Adaptive, Filter, Gallium Nitride, Reconfigurable, Surface Acoustic Wave, Thin-Film, Tunable**

I. Introduction

FOR many years now, acoustic filters such as surface acoustic wave (SAW) and bulk acoustic wave (BAW) devices have dominated the radio-frequency (RF) filtering applications due to their small size and low cost. Recently, their utilization has increased substantially in mobile phones where dozens of filters are required to accommodate carrier aggregation. This is a protocol which requires the use of many filters, each with a different center frequency and with a bandwidth that does not overlap with its neighbor. This forces designers to cram many filters into valuable area and with the number of filters single systems growing, it has generated an interest in the development of acoustic tunable filters [1]. Compounding interest on this topic is the emergence of wide-band adaptive RF front ends which require reconfigurable filters to attenuate undesired interference thus enabling the utilization of software-defined radios in congested and dynamic spectral environments [2].

There exist several approaches to realizing tunable filters. One strategy utilizes a bank of SAW transducers of different center frequencies which are controlled via switches to obtain a significant tunability of 25% [3], [4]. A popular technique at higher frequencies, SAW or BAW resonators are combined with variable capacitors to obtain a tunable center frequency of

Manuscript submitted for review April 30, 2020.
This work was partially supported by the National Science Foundation (NSF) EFRI 1641100 program.
The authors are with the Department of Electrical Engineering of Columbia University, New York, NY 10027 USA (e-mail: jab2361@columbia.edu).

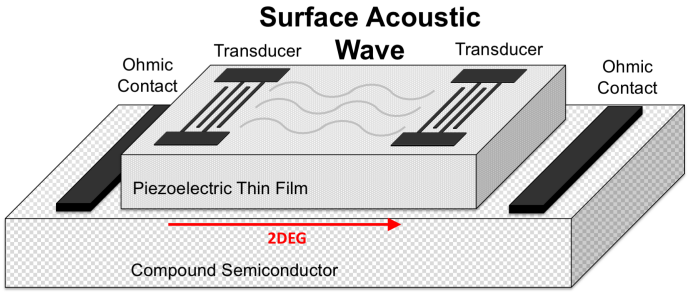

Fig. 1. Implementation of acoustoelectric filter composed of thin-film piezoelectric SAW filter fabricated on top of compound semiconductor.

up to 2.5 % [5]–[7]. The drawback of these implementations is that the addition of switches and varactors significantly increases the complexity and form factor. Thus, a simpler and more integrated device or architecture is desirable.

A potential solution exist using the acoustoelectric effect described in [8], where the propagation characteristics, namely the amplitude and phase velocity, of surface acoustic waves are modified by free carriers in a nearby semiconductor. Heavily researched in the 1960's and 1970's, this effect was originally investigated as a means to intrinsically amplify acoustic waves. Significant demonstrations of this effect were presented in [9], [10], where the authors obtained substantial amplification in a piezoelectric semiconductors CdS and GaAs crystals. Hampered by poor electromechanically coupling, efforts to improve performance focused on combining high-quality piezoelectric materials such as $LiNbO_3$ with high mobility bulk semiconductors such Si [11], [12] or thin-film semiconductors such as InSb [13] and CdSe [14] deposited on bulk piezoelectric crystals. While improved performance was achieved in terms of gain and stability, the devices suffered from large operating electric fields and high noise figure limiting their adoption in practical systems [15].

The amplitude of the acoustic wave is not the only aspect of its propagation affected by the acoustoelectric effect. When the free carrier concentration of the semiconductor is large enough to short out the penetrating electric field of the SAW, the acoustic velocity is decreased. This effect was demonstrated on two-dimensional electron gas (2DEG) of GaAs/AlGaAs where the GaAs also functions as the piezoelectric material [16], [17]. A hybrid $LiNbO_3$/AlGaAs/GaAs structure was demonstrated in [18] which exhibited a tunability of 0.172%. Recently, similar work has been extended to GaN/AlGaN heterostructures also utilizing the GaN buffer layer in an

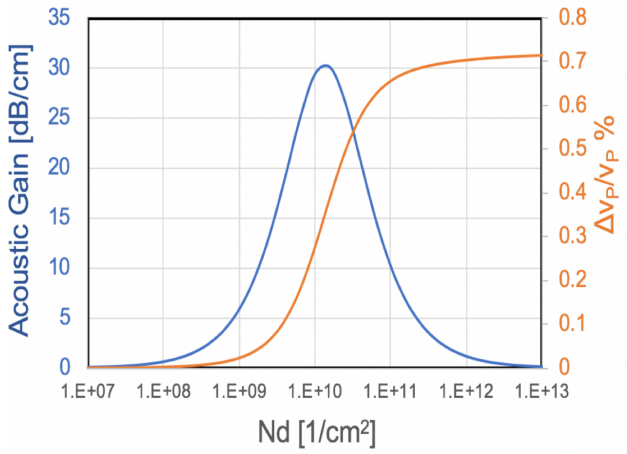

Fig. 2. Acoustic gain and phase velocity change due to the acoustoelectric effect according to normal mode theory model in [15] for $\boldsymbol{E = 500\frac{V}{cm}}$.

AlGaN/GaN epi for acoustic propagation while a metal-insulator-semiconductor (MIS) structure is used to tune the SAW response [19]. Unfortunately, the MIS structure results in a weak interaction only achieving a phase tunability of 0.07%. In [20], dual ZnO layers are grown on r-Al_2O_3 to achieve 0.44% relative frequency shift. A similar structure utilizes thin ZnO as a piezoelectric on top of n-type ZnO on GaN achieving a high tunability of .9% [21]. In this work, we demonstrate a ZnO on AlGaN/GaN heterostructure capable of achieving high tunability of 0.78% while also demonstrating control of the side-band rejection and bandwidth not previously observed due to an additional accumulation region.

II. Concept, Design, and Fabrication

A. Operating Principle

A diagram of the device is demonstrated in Fig. 1. A thin-film piezoelectric material is deposited and patterned on a compound semiconductor to obtain a high-quality SAW filter. The surface acoustic waves are induced on the piezoelectric film via the interdigitated transducers (IDT). Depending on the characteristics of the semiconductor, the effect can lead to amplification of the acoustic wave or in modulation of the phase velocity. Utilizing the normal mode theory model presented in [15] for the heterostructure structure in Fig. 1 with the material properties $\epsilon_P = 9.6\epsilon_0$, $\epsilon_S = 10.15\epsilon_0$, $\mu = 1600\frac{cm^2}{Vs}$, $V_P = 4000\frac{m}{s}$, $d_P = 1um$, and a $K^2_{eff} = 1\%$ where ϵ_P and ϵ_R are the permittivity of the piezoelectric and semiconductor materials respectively, μ is the carrier mobility of the semiconductor, V_P is the phase velocity of the acoustic wave, d_P is the thickness of the piezoelectric material, and K^2_{eff} is the electromechanical coupling of the piezoelectric material, the acoustic gain and change in phase velocity can be predicted as demonstrated in Fig. 2. As the acoustic waves propagates through the medium, it gives rise to an alternating electric field. If the free electrons are accelerated beyond the acoustic phase velocity, the acoustic waves are amplified due to an energy transfer that occurs when stress leads the strain. If the concentration is increased, a screening effect occurs causing a shorting of the electric field that results in power loss and piezoelectric stiffening.

This piezoelectric stiffening manifest itself in a decrease of phase velocity and since the center frequency of a SAW filter is given by

$$f_0 = \frac{v_0}{\lambda} \tag{1}$$

where λ is the periodicity of the transducers, this translates to a decrease in center frequency of the SAW filter. Thus, if a semiconductor is used to vary the concentration of free carriers, the degree of stiffening and thereby the center frequency can be actively modified.

B. Design Considerations

The change in attenuation and acoustic phase velocity from this effect by a nearby 2DEG is given by

$$\Gamma = \frac{\pi K^2_{eff}}{\lambda} \frac{\frac{\sigma_S}{\sigma_M}}{1 + (\frac{\sigma_S}{\sigma_M})^2} \tag{2}$$

and

$$\frac{\Delta v}{v_0} = \frac{K^2_{eff}}{2} \frac{1}{1 + (\frac{\sigma_S}{\sigma_M})^2} \tag{3}$$

TABLE I
Maximum tunability of the Multilayered configuration in Fig. 1 with different piezoelectric materials. Material parameters are taken from [22]–[24]

Piezoelectric Material	$V_{SAW}\frac{m}{s}$	K^2_{eff}	Attenuation dB/cm	Tunability
$LiNbO_3$	3890	5.5 %	.002	2.5 %
AlN	4500	.2 %	.01	.1 %
ZnO	3500	1.5%	6	.75 %

where σ_S is the sheet conductivity of the semiconductor, and σ_M is the relaxation conductivity and is expressed as $\sigma_M = V_0\epsilon_{eff}$ where ϵ_{eff} is the effective dielectric constant of the layered structure [17].

Table I shows the maximum tunability of different piezoelectric mediums an AlGaN/GaN epi with carrier density of $10^{13}cm^{-2}$ and mobility of $\mu = 1600\frac{cm^2}{Vs}$ where the conductivity is $\sigma_S = qN_D\mu$. As seen here, the tunability is dominated by the electromechanical coupling. Thus, the material with highest electromechanical coupling, $LiNbO_3$, will yield the highest tunability. However, $LiNbO_3$ cannot be easily grown on different substrates and only recently have thin-films been demonstrated on silicon through surface activation bonding [25]. AlN and ZnO are the most common materials used in this application since they can be sputtered on many different substrates. While AlN dominates the high frequency resonator application space, ZnO is capable of obtaining a larger electromechanical coupling leading to greater tunability. For this reason and its low thermal budget during deposition, ZnO is the material of choice for this work.

Critical piezoelectric characteristics such as acoustic phase velocity and electromechanical coupling are dispersive according to the thickness of the thin-film [26], [27]. This allows for the thickness of the piezoelectric to be chosen according to the

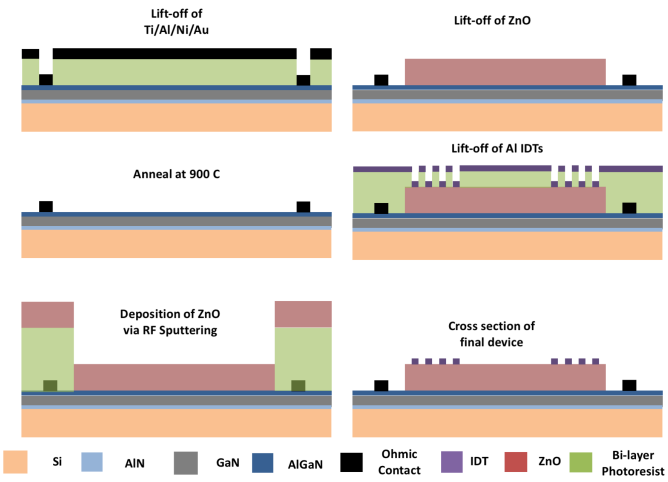

Fig. 3. Fabrication procedure for tunable SAW filter on an AlGaN/GaN Epi.

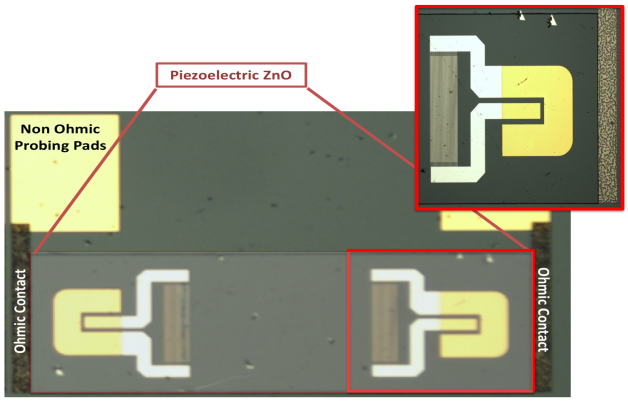

Fig. 4. Top view of final structure. Each IDT has 24 pairs of transducers with a pitch of 2 μm and 1mm apart.

desired frequency of interest without impacting the electrical properties of the semiconductor. From [27], a piezoelectric thickness to wavelength ratio, $\frac{h}{\lambda}$, greater than 0.1 should result in an electromechanical coupling above 1% and an acoustic velocity of in the 3800-4900 $\frac{m}{s}$ range. Considering this, a piezoelectric thickness of 1 um was chosen with a transducer and gap pitch of 2 um which corresponds to a $\frac{h}{\lambda}$ of 0.125. Utilizing the equivalent circuit model in [28] with the piezoelectric parameters $K^2_{eff} = 1\%$ and $V_0 = 4500\frac{m}{s}$, the number of pairs of the transducers were chosen to be 24 pairs with an aperture of 500um to obtain a transducer capacitance of 1.2 pF. Although mismatched, this is a high enough capacitance that can easily be resonated out by a series inductor. The transducers are 1mm apart to allow the placement of large DC probes directly on the ZnO. This was utilized instead of patterning an electrode on ZnO to avoid any further screening and mass loading of the acoustic wave.

C. Fabrication

Figure 3 illustrates the fabrication process used to construct the device. The AlGaN/GaN/AlN on silicon epi was obtained

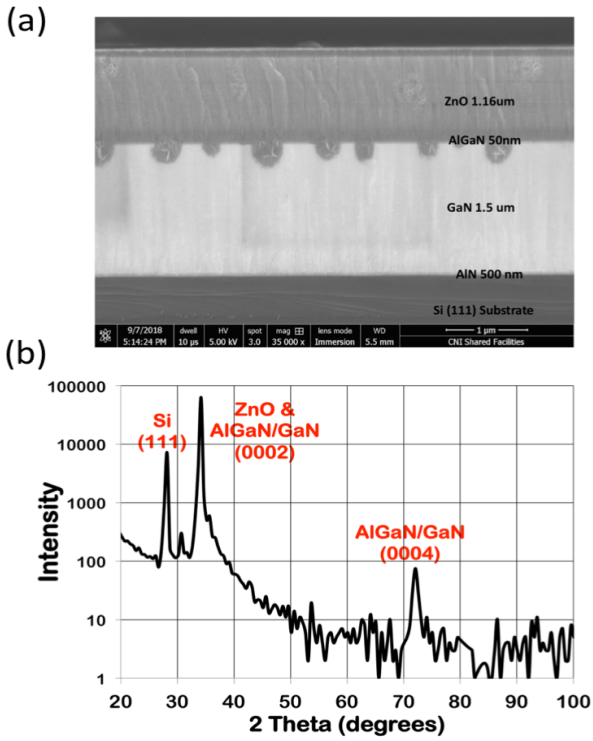

Fig. 5. (a) Scanning electron microscope image of the cross section of ZnO grown on AlGaN/GaN Epi. (b) X-Ray diffraction results demonstrating C-axis growth of ZnO on AlGaN/GaN.

as a donation from Raytheon Technologies and has an electron mobility of $\mu = 1570\frac{cm^2}{Vs}$ with 2DEG concentration of $N_D = 2.2 \times 10^{13} cm^{-2}$. A bi-layer of photoresist is patterned via photolithography and developed. Electron beam deposition is used to deposit Ti (400Å), Al (8000Å), Ni (400Å), and Au (8000Å) for the electrodes on the AlGaN. These are then annealed in a rapid thermal annealer at 900°C to form ohmic contacts to the 2DEG.

The ZnO is patterned using the lift-off method. A thick bi-layer of photoresist is patterned to define the piezoelectric area. RF sputtering is then used to deposit the ZnO at a rate of 0.7 Å/s for 5 hours. The sputtering conditions are the following: 150°C sample temperature, a power of 200W, a pressure of 2 mTorr, and an Ar to O_2 ratio of 1:1. The he device is then placed in remover PG solvent to lift-off the ZnO.

A scanning electron microscope (SEM) image of the cross-section of a sample processed in parallel to the device is shown in Fig. 5(a). The thickness of the film was verified to be 1.16 μm utilizing a thin-film spectrometer. The oval deformations are a result of stress during the cleaving process. Visually, the image is consistent with crystalline grown of the piezoelectric with clear appearances of grain boundaries similar to the epitaxially grown GaN layer underneath. However, to ensure piezoelectricity, X-ray diffraction (XRD) measurements were performed on the same sample. Fig. 5(b) depicts the XRD results which indeed show a C-axis crystal orientation of the resulting ZnO layer [29].

To finalize the structure, the IDTs are defined by patterning a bi-layer of photoresist by a laser writer and depositing 600Å

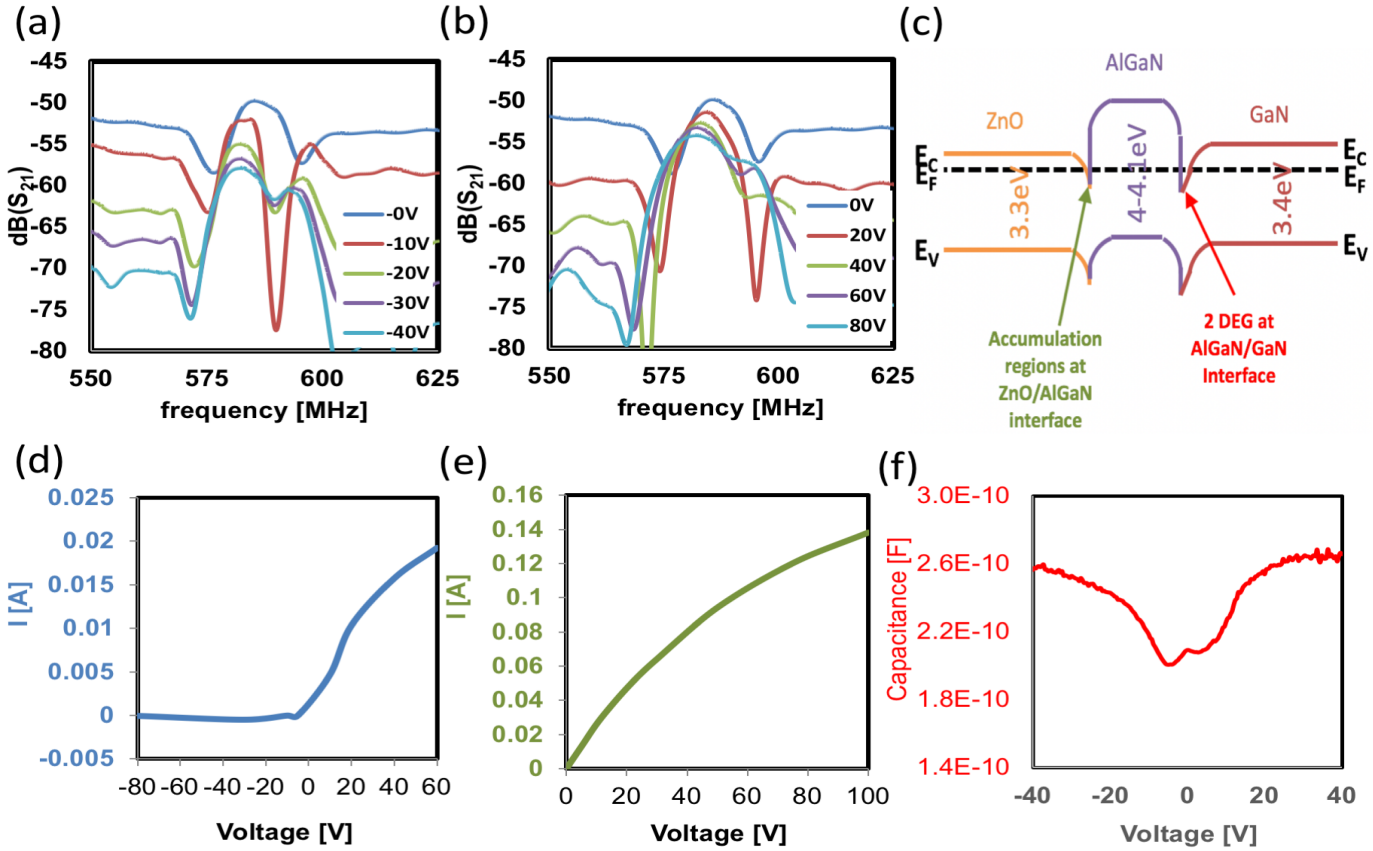

Fig. 6. (a) Forward transmission S-parameter, S_{21} of device biased at different voltages with a Config.2 setup. (b) Forward transmission S-parameter, S_{21}, of device biased at different voltages with a Config.2 setup. (c) Band diagram of ZnO/AlGaN/GaN heterostructure demonstrating the emergence of an accumulation layer at the Zno/AlGaN interface. (d) Current/Voltage relationship of vertically applied electric field on ZnO (Config. 2). (e) Current/Voltage relationship of vertically applied electric field on AlGaN/GaN ohmic contacts (Config. 1). (f) Capacitance/Voltage relationship of vertically applied electric field at 1KHz with a Config.2 setup.

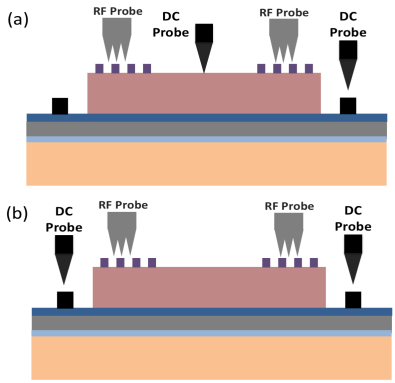

Fig. 7. (a) Configuration 1 (Confg. 1) where electric field is applied across ohmic contacts on AlGaN/GaN. (b) Configuration 2 (Confg. 2) where electric field is applied vertically on the ZnO and ohmic contact.

of Al. An additional lift-off lithographic step is used to deposit 1000Å of Au pads for the RF probing. Micrographs of the finalized structure are shown in Fig. 4. The IDTs have 24 pairs of fingers with a pitch of 1.5um and are 1mm apart.

III. Results and Discussion

A. Measurement Results

The device is measured under two different configurations as seen in Fig. 7 (a) and (b). In each one, the RF probes are applied to the probing pads connected to the transducers, however, the electric field is either applied vertically on the ZnO and on one of the ohmic contacts (Config. 1) or laterally across the ohmic contacts on the AlGaN/GaN (Config. 2). The transmission S-parameters, S_{21}, under different voltage biases for both configurations are shown in Fig. 6(a) and (b). Under a 0V bias in Fig. 6(a), the device shows a center frequency of 586 MHz, indicating an acoustic phase velocity of 4544 $\frac{m}{s}$. As the bias grows more negative, the insertion loss increases and the side-band rejection and bandwidth also increase, however, very little change occurs in the center frequency of the device. Under the Config. 2 setup in Fig. 6(b), the the same effect appears, however, the center frequency of the filter is also down-shifted. This suggest that the acoustoelectric effect is dominated by the 2DEG at AlGaN/GaN interface while the effect observed during the vertically applied electric field can be explained by the formation of an accumulation layer at the ZnO/AlGaN interface as seen in Figure 6(c). This is further supported by the current voltage relationships of a vertically applied electric field across the ZnO, Figure 6 (d), and a

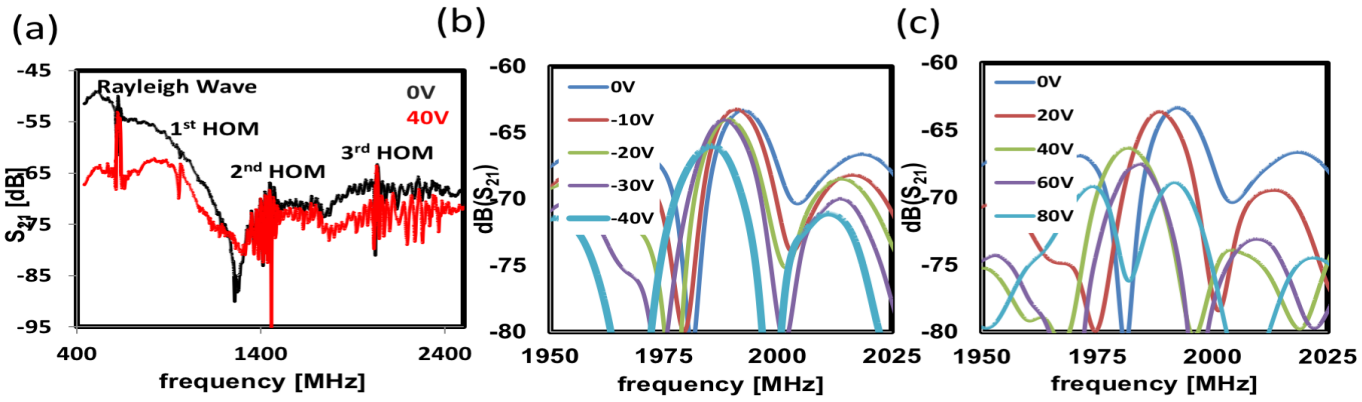

Fig. 8. (a) Forward transmission S-parameter, S_{21} showing wide-band response of the device under 0V and 40V bias in a Config.2 setup. (b) Forward transmission S-parameter, S_{21} response of the 3rd HOM under different bias in a Config.1 setup. (c) Forward transmission S-parameter, S_{21} response of the 3rd HOM under different bias in a Config.2 setup.

laterally applied electric field across the AlGaN/GaN ohmic contacts, Figure 6 (e). As the vertical electric field is applied very little current is observed at reverse bias, but as the voltage approaches 0 volts and beyond, the Schottky barrier formed by the probe and the ZnO is forward biased and a large current flows from the surface of the ZnO to the ohmic contact on the AlGaN/GaN.

To investigate how much the vertically applied electric field can gate the 2DEG in the AlGaN/GaN interface, an impedance analyzer was used to measure the capacitance-voltage (CV) relationship. Fig. 6 (f) demonstrates the CV relationship of the vertically applied electric field at 1KHz. While some electrostatic control is observed, it is very weak, thus verifying that the acoustoelectric effect observed is mostly due to the increase in carrier concentration in the 2DEG due to the laterally applied electric field on the ohmic contacts.

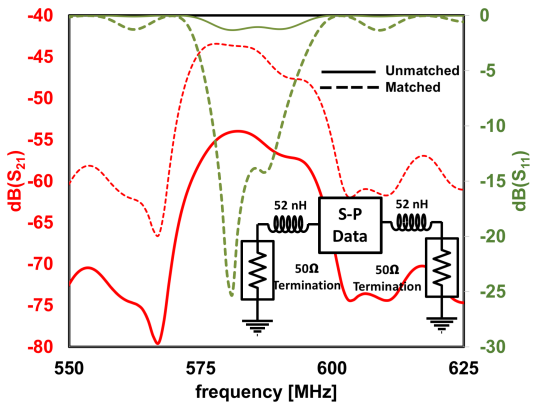

Fig. 9. S_{21} and S_{11} S-parameters for SAW response at a 80 volt bias under Config. 1 setup for unmatched raw data and matched data in simulation software. Circuit shows the configuration utilized to match both ports. Output match, S_{22}, is nearly identical to S_{11} so it is not included in the plot.

B. Effect on Higher Order Modes

Higher order modes (HOM) are known to be present in c-axis ZnO thin-film SAW devices [23], [27] and are often the focus of the design instead of the fundamental Rayleigh wave since they can possess higher electromechanical coupling and phase velocities. Therefore, it is of interest to examine the if these higher modes also exhibit similar characteristics due to the acoustoelectric effect. Figure 8 (a) demonstrates the wide band response of the filter biased at 0V and 40V under Config.2. Since the response of the 1st and 2nd order modes are obscured and difficult to analyze, the focus of the discussion will be on the 3rd mode. Fig. 8 (b) demonstrates the response of the 3rd HOM under a Config.1 setup. Unlike the fundamental Rayleigh wave, the effect on the center frequency is evident reaching a total difference of 0.35% while effects on side-band rejection and bandwidth are very little. Under the Config. 2 measurement setup, Fig. 8 (c), the effect is much more pronounced reaching a total difference of 0.556% from the center frequency at a 40 V bias. Thus, similarly to the fundamental mode, the acoustoelectric effect is stronger under Config.2 biasing.

C. Discussion

Fig. 10 (a) and (b) summarize the change in insertion loss and phase velocity due to the acoustoelectric effect versus voltage bias under both configuration setups for the fundamental and 3rd HOM. Both demonstrate a general trend in insertion loss as it degrades by up to 4dB in as the bias is increased. Under Config. 1, the phase velocity is decreased by 0.074% the original value when no bias is applied while the 3rd HOM is shifted by 0.23%. When biased under Config. 2, the phase velocity is decreased by up to 0.78% which corresponds to a 4.64 MHz decrease in center frequency for the fundamental mode. For the 3rd order mode, the maximum change of 0.556% or 11.1 MHz is achieved at a bias of 40V, while beyond 60V the center frequency becomes difficult to identify. While the effect is present in Config.1, the interaction is stronger in a Config. 2 setup signifying that it is dominated by the 2DEG. Additionally, a considerable amount of power can be drawn in the Config. 2 setup that will result in some heating of the ZnO thin-film. Since the thermal coefficient of frequency (TCF) of thin-film ZnO is $-42\frac{ppm}{^\circ C}$ [29], the frequency shift is likely dominated by the acoustoelectric

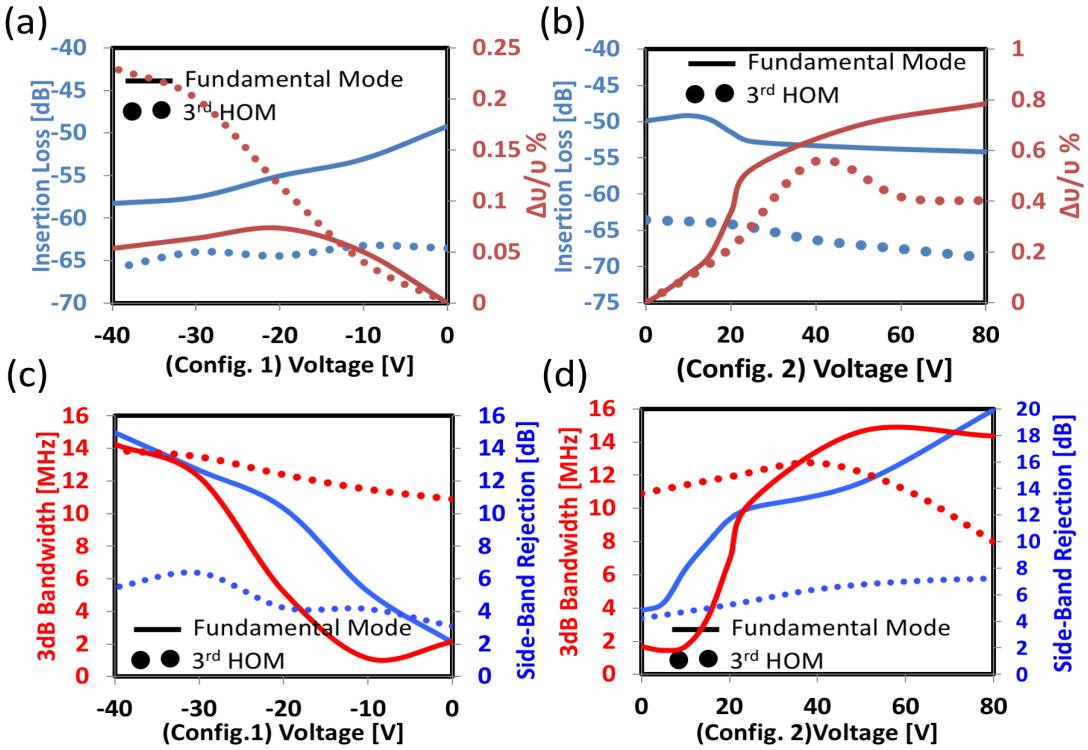

Fig. 10. (a) Insertion loss at the center frequency and change in phase velocity versus applied voltage for both fundamental and 3rd HOM in a Config. 1 setup. (b) Insertion loss at the center frequency and change in phase velocity versus applied voltage for both fundamental and 3rd HOM in a Config. 2 setup. (c) Bandwidth and Side-Band Rejection versus applied voltage for fundamental and 3rd HOM in a Config. 1 setup. (d) Bandwidth and Side-Band Rejection versus applied voltage for fundamental and 3rd HOM in a Config. 2 setup. The side band rejection ratio is calculated by comparing the insertion loss at the center frequency to the insertion loss of the left side-lobe.

effect. This is further supported by the results under the Config. 2 setup where very little to no current is drawn.

An interesting feature of this device is the effect the additional accumulation layer has on filtering metrics such as the side-band rejection and bandwidth. As seen in Fig. 10 (c) and (d), the side-band rejection and bandwidth of both modes increase with bias. While this particular measurement is performed without the application of a vertical electric field, the same behavior can be seen in Fig. 10 (d). As discussed previously, this is due to the formation of an accumulation layer at the ZnO/AlGaN interface which acts as conductive path which shields the SAW. By applying a vertical electric field on the ZnO, a high negative bias depletes this region of carriers. The same effect is achieved by applying a bias laterally across the ohmic contact of the AlGaN/GaN. As current increases in the 2DEG, the carrier concentration in the 2DEG causes a depletion at the ZnO/AlGaN interface since the 2DEG is very close to the surface. Thus, why the 2DEG also dominates the acoustoelectric effect as well.

This effect is can be observed in simulation using the small-signal equivalent circuit demonstrated in Fig. 11 (a). A resistor is used to model the ohmic contact and the 2DEG in the AlGaN/GaN interface which is connected to a voltage-controlled current source which acts as the accumulation region in the ZnO/GaN interface. The current source is capacitively coupled to the IDTs on the ZnO. These capacitances represent the reverse bias capacitance of the ZnO/AlGaN junction. The piezoelectric properties of the ZnO are modeled by the equivalent circuit reported in [28]. Figure 11 (b) demonstrates the simulation results at different applied biases from 0V to 80V in 10V steps. This simulation replicates the behavior seen in measurements as the voltage is increased thus providing empirical verification of the mechanisms behind the effect.

While the acoustoelectric effect is strong for fundamental and higher modes of propagation, the performance of the piezoelectric material leaves quite a bit to be desired, specifically in terms of the insertion loss. This is in part due to the large input and output impedance mismatch at the RF ports. To investigate how much improvement could be made by properly matching the transducers, the s-parameter data was imported into simulation software (Keysight Advances Design System) where series inductors of 52 nH were added to both input and output. Fig. 9 demonstrates an improvement of 9.8 dB by properly matching the input and output impedances. Although this is significant, the insertion is still substantial. Other improvements could be made by lowering the impedance of the transducers by increasing the aperture size or increasing the number of pairs, albeit the latter will decrease the bandwidth of the filter response.

While ZnO suffers from high propagation loss, these have been reported to be in the $6.5\frac{dB}{cm}$ range and since the gap between transducers in work is 1 mm, a big improvement in narrowing the gap is not expected [30]. Some improvement could be obtained by increasing the ZnO thickness so that $\frac{h}{\lambda} > 0.125$. Obtaining a $\frac{h}{\lambda}$ between 0.15 and 0.2 has been shown to maximize the electromechanical coupling of

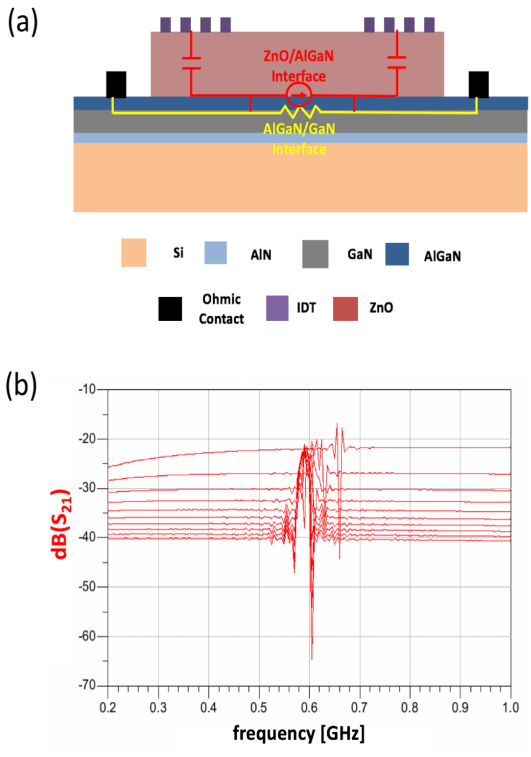

Fig. 11. (a) Cross-section and equivalent circuit to model the effect of the extra accumulation layer on the ZnO/AlGaN interface. (b) Simulation results in ADS using equivalent circuit model.

ZnO albeit at the cost of reduced phase velocity [29]–[31]. Significant improvements have also been made by utilizing ZnO sputtering targets doped with Nickel [31] or Manganese [32]. The doping of the ZnO offers a very interesting path in future studies since this would impact the creation of the accumulation layer in the ZnO/AlGaN interface depending on the resulting polarity.

Significant improvements can be made by utilizing a higher electromechanical coupling material such as $LiNbO_3$. While integrating $LiNbO_3$ with other materials has been difficult historically, recent techniques utilizing surface activated bonding have been successfully demonstrated to yield very high K^2_{eff} on silicon substrates [25], [33]. Perhaps an even more interesting path forward is to investigate Scandium Aluminum Nitride (ScAlN) which as been demonstrated to be a outstanding piezoelectric material and semiconductor [34]–[36]. This material can be leveraged to improve on this device significantly.

IV. Conclusion

In this article, a reconfigurable SAW filter has been demonstrated on ZnO/AlGaN/GaN heterostructure. While the insertion loss and center frequency is governed by the acousto-electric effect between the acoustic waves on the ZnO and the carriers in the 2DEG at the AlGaN/GaN interface with a high tunability of 0.78% for the fundamental mode and 0.556% for the 3rd higher order mode, the emergence of an additional accumulation layer at the ZnO/AlGaN interface allows for the control of the bandwidth as well as the side-band rejection ratio. Although the insertion loss of the device must be improved for practical systems, this device signifies that these heterostructures are great candidates for reconfigurable SAW filters. By properly engineering the junction interfaces, more functionality can be obtained along with tunability.

References

[1] S. Mahon, "The 5g effect on rf filter technologies," *IEEE Transactions on Semiconductor Manufacturing*, vol. 30, no. 4, pp. 494–499, 2017.

[2] Defense Advances Research Projecs Agecy, "Broad Agency Announcement Wideband Adaptive RF Protection (WARP) Microsystems Technology Office," pp. 1–47, 2020.

[3] Jiahua Zhu, N. W. Emanetoglu, Yicheng Lu, J. A. Kosinski, and R. A. Pastore, "A multi-idt input tunable surface acoustic wave filter," *IEEE Transactions on Ultrasonics, Ferroelectrics, and Frequency Control*, vol. 48, no. 5, pp. 1383–1388, 2001.

[4] Jiahua Zhu, N. W. Emanetoglu, Yicheng Lu, J. A. Kosinski, R. Pastore, and A. Lepore, "A prototype of tunable surface acoustic wave filter," in *1999 IEEE Ultrasonics Symposium. Proceedings. International Symposium (Cat. No.99CH37027)*, vol. 1, 1999, pp. 47–50 vol.1.

[5] A. Konno, H. Hirano, M. Inaba, K. Y. Hashimoto, M. Esashi, and S. Tanaka, "Tunable surface acoustic wave filter using integrated micro-electro- mechanical-system based varactors made of electroplated gold," *Japanese Journal of Applied Physics*, vol. 52, no. 7 PART 2, pp. 0–5, 2013.

[6] M. Inaba, T. Omori, and K. Y. Hashimoto, "A Configuration of widely tunable surface acoustic wave filter," *Japanese Journal of Applied Physics*, vol. 52, no. 7 PART 2, pp. 3–7, 2013.

[7] T. Komatsu, K. Y. Hashimoto, T. Omori, and M. Yamaguchi, "Tunable radio-frequency filters using acoustic wave resonators and variable capacitors," *Japanese Journal of Applied Physics*, vol. 49, no. 7 PART 2, 2010.

[8] R. H. Parmenter, "The acousto-electric effect," *Phys. Rev.*, vol. 89, pp. 990–998, Mar 1953. [Online]. Available: https://link.aps.org/doi/10.1103/PhysRev.89.990

[9] A. R. Hutson, J. H. McFee, and D. L. White, "Ultrasonic amplification in cds," *Phys. Rev. Lett.*, vol. 7, pp. 237–239, Sep 1961. [Online]. Available: https://link.aps.org/doi/10.1103/PhysRevLett.7.237

[10] S. Ludvik and C. F. Quate, "Amplification of surface shear-wave mode in gaas," *Journal of Applied Physics*, vol. 43, no. 9, pp. 3619–3622, 1972. [Online]. Available: https://doi.org/10.1063/1.1661777

[11] K. M. Lakin and H. J. Shaw, "Surface wave delay line amplifiers," *IEEE Transactions on Microwave Theory and Techniques*, vol. 17, no. 11, pp. 912–920, 1969.

[12] K. M. Lakin, J. H. Collins, and P. J. Hagon, "100 mhz surface acoustoelectric amplifier exhibiting stable terminal gain with dc drift field," *Proceedings of the IEEE*, vol. 57, no. 4, pp. 740–742, 1969.

[13] L. A. Coldren and G. S. Kino, "The insb on a piezoelectric rayleigh wave amplifier," *IEEE Transactions on Electron Devices*, vol. 21, no. 7, pp. 421–427, 1974.

[14] H. Hanebrekke and K. A. Ingebrigtsen, "Acoustoelectric amplification of surface waves in structure of cadmium-selenide film on lithium niobate," *Electronics Letters*, vol. 6, no. 16, pp. 520–521, 1970.

[15] G. S. Kino, "Acoustoelectric interactions in acoustic surface wave devices," *Proceedings of the IEEE*, vol. 64, no. 5, pp. 724–748, 1976.

[16] C. Rocke, S. Manus, A. Wixforth, M. Sundaram, J. H. English, and A. C. Gossard, "Voltage tunable acoustoelectric interaction in gaas/algaas heterojunctions," *Applied Physics Letters*, vol. 65, no. 19, pp. 2422–2424, 1994. [Online]. Available: https://doi.org/10.1063/1.112694

[17] A. Wixforth, J. Scriba, M. Wassermeier, J. P. Kotthaus, G. Weimann, and W. Schlapp, "Surface acoustic waves on gaas/al_xga_{1-x}as heterostructures," *Phys. Rev. B*, vol. 40, pp. 7874–7887, Oct 1989. [Online]. Available: https://link.aps.org/doi/10.1103/PhysRevB.40.7874

[18] M. Rotter, W. Ruile, A. Wixforth, and J. P. Kotthaus, "Voltage controlled saw velocity in gaas/linbo/sub 3/-hybrids," *IEEE Transactions on Ultrasonics, Ferroelectrics, and Frequency Control*, vol. 46, no. 1, pp. 120–125, 1999.

[19] J. Pedrós, F. Calle, R. Cuerdo, J. Grajal, and Z. Bougrioua, "Voltage tunable surface acoustic wave phase shifter on algan/gan," *Applied Physics Letters*, vol. 96, no. 12, p. 123505, 2010. [Online]. Available: https://doi.org/10.1063/1.3353971

[20] J. Zhu, Y. Chen, G. Saraf, N. W. Emanetoglu, and Y. Lu, "Voltage tunable surface acoustic wave phase shifter using semiconducting/piezoelectric zno dual layers grown on r-al2o3," *Applied Physics Letters*, vol. 89, no. 10, p. 103513, 2006. [Online]. Available: https://doi.org/10.1063/1.2347695

[21] R. Li, P. I. Reyes, S. Ragavendiran, H. Shen, and Y. Lu, "Tunable surface acoustic wave device based on acoustoelectric interaction in zno/gan heterostructures," *Applied Physics Letters*, vol. 107, no. 7, p. 073504, 2015. [Online]. Available: https://doi.org/10.1063/1.4928724

[22] M. Clement, L. Vergara, J. Sangrador, E. Iborra, and A. Sanz-Hervás, "Saw characteristics of aln films sputtered on silicon substrates," *Ultrasonics*, vol. 42, no. 1, pp. 403 – 407, 2004, proceedings of Ultrasonics International 2003. [Online]. Available: http://www.sciencedirect.com/science/article/pii/S0041624X04000411

[23] S. Ghosh, M. A. Hollis, and R. J. Molnar, "Acoustoelectric amplification of rayleigh waves in low sheet density algan/gan heterostructures on sapphire," *Applied Physics Letters*, vol. 114, no. 6, p. 063502, 2019. [Online]. Available: https://doi.org/10.1063/1.5080450

[24] M. Fraga, H. Furlan, R. Pessoa, and M. Massi, "Wide bandgap semiconductor thin films for piezoelectric and piezoresistive mems sensors applied at high temperatures: An overview," *Microsystem Technologies*, vol. 20, pp. 9–21, 12 2013.

[25] S. Ballandras, E. Courjon, F. Bernard, T. Laroche, A. Clairet, I. Radu, I. Huyet, A. Drouin, and E. Butaud, "New generation of saw devices on advanced engineered substrates combining piezoelectric single crystals and silicon," in *2019 Joint Conference of the IEEE International Frequency Control Symposium and European Frequency and Time Forum (EFTF/IFC)*, 2019, pp. 1–6.

[26] T. Yamamoto, T. Shiosaki, and A. Kawabata, "Characterization of zno piezoelectric films prepared by rf planar-magnetron sputtering," *Journal of Applied Physics*, vol. 51, no. 6, pp. 3113–3120, 1980. [Online]. Available: https://doi.org/10.1063/1.328100

[27] N. Emanetoglu, C. Gorla, Y. Liu, S. Liang, and Y. Lu, "Epitaxial zno piezoelectric thin films for saw filters," *Materials Science in Semiconductor Processing*, vol. 2, no. 3, pp. 247 – 252, 1999. [Online]. Available: http://www.sciencedirect.com/science/article/pii/S1369800199000220

[28] K. Nakamura, "A simple equivalent circuit for interdigital transducers based on the coupled-mode approach," *IEEE Transactions on Ultrasonics, Ferroelectrics, and Frequency Control*, vol. 40, no. 6, pp. 763–767, 1993.

[29] N. Emanetoglu, C. Gorla, Y. Liu, S. Liang, and Y. Lu, "Epitaxial zno piezoelectric thin films for saw filters," *Materials Science in Semiconductor Processing*, vol. 2, no. 3, pp. 247 – 252, 1999. [Online]. Available: http://www.sciencedirect.com/science/article/pii/S1369800199000220

[30] A. H. Weber, G. Weiss, and S. Hunklinger, "Comparison of rayleigh and sezawa wave modes in zno-sio/sub 2/-si structures," in *IEEE 1991 Ultrasonics Symposium,*, 1991, pp. 363–366 vol.1.

[31] H. Ieki, H. Tanaka, J. Koike, and T. Nishikawa, "Microwave low insertion loss saw filter by using zno/sapphire substrate with ni dopant," in *1996 IEEE MTT-S International Microwave Symposium Digest*, vol. 2, 1996, pp. 409–412 vol.2.

[32] J. T. Luo, P. Fan, F. Pan, F. Zeng, D. P. Zhang, Z. H. Zheng, G. X. Liang, and X. M. Cai, "Effects of mn-doping on surface acoustic wave properties of zno films," *physica status solidi (RRL) – Rapid Research Letters*, vol. 6, no. 11, pp. 436–438, 2012. [Online]. Available: https://onlinelibrary.wiley.com/doi/abs/10.1002/pssr.201206381

[33] J. Zou, F. Iliev, R. B. Hammond, S. Samadian, P. J. Turner, V. Yantchev, N. O. Fenzi, and V. Plessky, "Low-loss, high-frequency and large-coupling sh saw resonators based on sin/linbo3/si," in *2018 IEEE International Ultrasonics Symposium (IUS)*, 2018, pp. 1–4.

[34] K. Hashimoto, S. Tanaka, and M. Esashi, "Tunable rf saw/baw filters: Dream or reality?" in *2011 Joint Conference of the IEEE International Frequency Control and the European Frequency and Time Forum (FCS) Proceedings*, 2011, pp. 1–8.

[35] A. Ansari, "Single crystalline scandium aluminum nitride: An emerging material for 5g acoustic filters," in *2019 IEEE MTT-S International Wireless Symposium (IWS)*, 2019, pp. 1–3.

[36] T. E. Kazior, E. M. Chumbes, B. Schultz, J. Logan, D. J. Meyer, and M. T. Hardy, "High power density scaln-based heterostructure fets for mm-wave applications," in *2019 IEEE MTT-S International Microwave Symposium (IMS)*, 2019, pp. 1136–1139.